Electrical conductivity of CdS films for gas sensing: selectivity properties to alcoholic chains

A. Giberti[*1,2], D. Casotti[1], G. Cruciani[1], A. Gaiardo[1], V. Guidi[1,2,3], C. Malagù[1,3], G. Zonta[1]

[1] Department of Physics and Earth Science, University of Ferrara, Via Saragat 1/c, 44122 Ferrara, Italy
[2] MIST E-R s.c.r.l., Via P. Gobetti 101, 40129 Bologna, Italy
[3] CNR-INO – Istituto Nazionale di Ottica, Largo Enrico Fermi 6, 50124 Firenze, Italy

Abstract

Nanophased cadmium sulfide powder was synthesized with a simple route and characterized with thermal, structural and morphological analysis. Conductometric gas sensors based on synthesized CdS were fabricated by means of screen-printing technology and their sensing properties were tested on a selection of alcohols, aldehydes, ketones and other gaseous compounds. We found that, at working temperature of 300°C, the CdS films show a strong selectivity vs alcohols, proving that they can selectively detect alcohols in mixtures where aldehydes and other interferers are present. A possible sensing mechanism that accounts for this selectivity, as well as for the sensitivity to the length of the alcoholic chain, was proposed.

Keywords: gas sensor, cadmium sulfide, alcohols sensing, nanostructured CdS film

* Corresponding author. Tel. +39 0532 974270
Email address: giberti@fe.infn.it

1. Introduction

Cadmium sulphide (CdS) is a wide gap semiconductor (E_g = 2.40 eV), widely used in many fields of science and technology due to its interesting chemical and physical properties. In particular, this material shows piezoelectricity, photoconductivity, chemoresistivity and electroluminescence. Owing to these properties, CdS-based devices can be employed as solar cells, photoresistors, piezoelectric transducers and gas sensors [1-4]. A recent interesting example of a CdS-based gas sensor is reported in [5], where it is shown that a luminescent reaction between alcohol molecules and CdS surface can occur, and it can be employed as basic mechanism for alcohols-selective luminescent gas sensors. Furthermore, as also shown in this work, nanostructured CdS-based films have great potentialities as conductometric gas sensors. However, very few studies can be found in literature about this application of CdS. The majority of scientific papers regarding conductometric gas sensors are focused on metal oxides [6-13], even though there are other classes of materials that show chemoresistive properties [14].

In a recent work on nanostructured CdS films, we evidenced that the surface chemistry, responsible for chemoresistive properties, can be resonantly photo-activated at room temperature, proving their ability to operate as conductometric gas sensors at room temperature under proper electromagnetic irradiation [15]. In the present work, instead, we studied their behaviour under thermal activation. We synthesized CdS nanopowder and we characterized it determining the crystal phase(s), estimating the crystal size, and studying the thermal behaviour. Then, we deposited the CdS powder onto alumina substrates to build conductometric CdS-based gas sensors. We found that, depending on working temperature, the as-prepared devices can be efficiently employed to selectively detect alcohols in complex mixtures.

2. Experimental

2.1 Synthesis of CdS powder and film deposition

All chemicals employed in this work were from Sigma Aldrich. CdS nanoparticles were synthesized by precipitation route in water solution at room temperature and atmospheric pressure. In a typical preparation, 2.66 g of cadmium acetate hydrate (10 mmol) and o-diaminobenzene (2.16 g, 20 mmoles) were dissolved in water and stirred for two hours. Then, 20 mmol of thioacetamide (1.5 g) were added to the solution and the mixture was stirred again for six hours. A yellow-orange precipitate was formed. It was isolated by vacuum filtration and washed several times with water and methanol. Finally, the product was dried for 4 hours at 40°C. The synthesis was carried out without (sample S1), and with (sample S2) 20 mmol of o-diaminobenzene as complexing agent.

The sensing layers were realized by adding a proper amount of organic vehicles to the CdS powder, in order to obtain a screen-printing paste with the right viscosity for the deposition onto alumina substrates [8]. The latter are equipped with pre-deposited metal electrodes to provide the voltage to the film and with a heater on the back-side to set the desired working temperature. Then, the screen-printed films were subjected to thermal stabilization at 180°C in a muffle oven for 12 hours in air, to allow the evaporation of organic vehicles. Then, the substrate was mounted on a suitable support to be interfaced with the electronic measuring system.

2.2 Characterizations

Both the powder and the films were analyzed with Scanning Electron Microscopy and Energy Dispersive X-Ray spectroscopy (SEM-EDX spectroscopy) techniques, by means of a Zeiss EVO 40 microscope with an acceleration voltage of 30 kV, to investigate the morphology and chemical composition of the obtained material.

The as-synthesized CdS nanopowder and thermal processed powder were characterized by power X-Ray Diffraction (XRD) using a Bruker D8 Advance diffractometer with an X-ray tube operating at 40 kV and 40 mA, and equipped with a Si(Li) solid-state detector (SOL-X) set to

measure CuKα1,2 radiation. As-synthesized samples and powders after thermal treatments were side-loaded on an aluminum holder and zero-back ground holder respectively. Measuring conditions were 5 to 95 °2θ range, 0.02 °2θ scan rate, counting time per step 4 and 6 s for as synthesized and thermally treated nanopowders, respectively. The phase identification was achieved by search-match using the EVA v.14.0 program by Bruker and the Powder Diffraction File database (PDF) v. 9.0.133. The crystallite size of the as synthesized nanopowder was determined by the Rietveld method as implemented in TOPAS v.4.1 program by Bruker AXS [16]. The fundamental parameters approach was used for the line-profile fitting [17-19]. The determination of crystallite size by TOPAS was accomplished by the Double-Voigt approach [20]. In particular, the crystallite size was calculated as volume-weighted mean column heights based on integral breadths of peaks.

The thermogravimetric (TG/DTG/DTA) curves of the screen-printing paste were recorded using a Netzsch 409 PC Luxx TG/DTA thermal analyzer. About 70 mg of samples were filled in a nickel crucible and analyzed in the range 20-800 °C, with heating rate of 10 °C min^{-1} under air flow of 20 ml h^{-1}.

The optoelectronic properties of the synthesized material were investigated by UV-Vis absorption measurements in the range 300 – 900 nm (Cary 50 Varion, Virtual double-radius), using dimethyl sulfoxide both as reference and solvent. The cuvette was in quartz and the optical path of 1 cm.

2.3 Gas measurements

The electrical conductance of the CdS sensors was measured in a test chamber using the flow-through technique. The sensors were kept at their working temperature and under a flow of dry air for few hours before the gas measurements, in order to allow the surface of the CdS grains to reach a thermodynamic steady state. Air and gases were from certified bottles, and the injection in the chamber occurred by means of a PC-driven mass-flow-controller. The conductance of the films

were constantly monitored during gas measurements through proper electronics interfaced to a data-acquiring system.

3. Results and discussion

3.1 Results of characterizations

In order to check the effect of o-diaminobenzene as complexing agent, EDX analysis was performed on both samples S1 and S2. It resulted that the synthesis performed without the complexing agent led to a product with poor purity due to oxygen and carbon residuals, while the synthesis performed with the complexing agent led to a strong improvement of the sample purity (higher than 99%), with almost perfect stoichiometry and lower grain dimensions. For this reason we chose to employ sample S2 for the preparation of the chemoresistive films. The results of SEM-EDX measurements on the sample S2 are shown in Fig. 1. In the SEM image, it can be observed the spherical morphology of the grains, with an average grain size around 100 nm, while in the inlay we reported a plot of the EDX peaks and the result of the chemical analysis. This experiment has highlighted the importance of chelating agents, such as o-diaminobenzene, in the synthesis of crystalline nanoparticles. O-diaminobenzene acts as chelating ligand with Cd^{2+} ions to form a complex, and thioacetamide is readily decomposed and acts as sulfur source, generating S^{2-} ions. As known in literature, the formation of an intermediate metal-ligand complex is important to inhibit the grains growth, to enhance particle stabilization and to improve the optical properties [21]. Further characterizations were performed on sample S2 only.

The results of XRD measurements of the synthetized nanopowder are shown in Fig. 2. From the analysis of the phase composition, as described in Experimental Section, it turns out that the material is monophasic and the peaks correspond to the cubic polymorph of cadmium sulfide, β-CdS/hawleyite (space group F-43m), assuring us that the synthesis method yielded very high purity CdS. The determined crystallite size resulted 2.59 ± 0.14 nm. In Fig. 3 it is reported the TG/DTG/DTA analysis performed on the screen-printing paste, in which we can observe an

exothermic peak at about 200 °C, due to the loss of organic vehicle. The TG curve shows that no significant changes occur to the material up to about 500°C, this indicating stoichiometric and morphological stability. Above a temperature of about 550°C, a weight gain of the sample can be noticed. To figure out this phenomenon, a XRD analysis was performed after the thermogravimetric measurement. The corresponding XRD pattern is shown in Fig. 4, where the presence of cadmium oxide sulfate ($Cd_3O_2SO_4$), cadmium sulfate ($CdSO_4$) and cadmium oxide (CdO) crystalline phases can be observed. The formation of $Cd_3O_2SO_4$ and $CdSO_4$, in particular, explains the weight gain above 550°C.

UV-Vis absorption measurements are shown in Fig. 5. It can be noticed an absorption band in the ultraviolet-visible range between about 350 and 510 nm, peaked slightly below 450 nm. This absorption peak is blue-shifted compared to the characteristic peak at 515 nm of bulk cubic cadmium sulfide (II), due to the electronic transitions. This phenomenon is known as "quantum size effect" [22,23].

3.2 Gas performing results

A series of experiments was scheduled, focusing on different categories of gases. The aim was to have an insight of the possible mechanisms by observing the effect on the activity of CdS surface of gas molecules with important chemical differences. To this end, we chose methanol, ethanol and n-butanol as alcohols, acetone as ketone, acetaldehyde as aldehyde, sulfur dioxide (SO_2) as anhydride, molecular hydrogen as low-reactive compound, nitrogen dioxide (NO_2) as oxidizing agent and methane as hydrocarbon. The concentrations were chosen in a range 1-20 ppm, apart from methane, for which 2500 ppm is a rather low concentration.

The sensors were tested at working temperatures of 250, 300 and 350°C. The gas performance was evaluated by the electrical response of the sensors, defined as

$$R = \begin{cases} \left(G_{gas} - G_{air}\right)/G_{air} & \text{for a conductance increase (reducing gas)} \\ \left(G_{gas} - G_{air}\right)/G_{gas} & \text{for a conductance decrease (oxydizing gas)} \end{cases}, \quad (1)$$

where G_{gas} and G_{air} are the steady-state conductances in gas and in air, respectively. It follows from definition of Eq. (1) that R is zero for a gas that leaves the conductance unchanged, it is positive for reducing gases and negative for oxidizing gases.

Very different results were found for alcohols compared to all other gases, at all working temperatures. The responses of a typical CdS sensor, to the indicated gas concentrations, are reported in Table I, and their absolute values are shown in the histogram of Fig. 6. An important fact, common to all working temperatures, was that, in the case of alcohols, the longer the alcoholic chain the higher the sensor's response. Injection of methanol into the test chamber caused a huge, rapid conductance increase (few minutes), followed by a slower decrease, which ended in a modest conductance increase (few units). Response to ethanol, instead, required only few minutes to reach a steady state, with a huge response enhancement with respect to methanol (more than one order of magnitude). With n-butanol the behavior was very similar, but with an even higher response. 250°C was the only temperature in which we observed a reducing behavior in the case of alcohols and an oxidizing behavior in the case of all other gases. The response to alcohols increased from 1 for methanol to 10 for ethanol and 20 for n-butanol, while for all other gases we recorded very low responses (absolute value about lower than 1, except for NO_2, which yielded $|R| \approx 10$). At 300°C we observed a reducing behavior for all gases, with $R \approx 7$ for methanol, 60 for ethanol and 90 for n-buthanol. The other categories of gases produced negligible responses (lower than 1), except for acetaldehyde, for which $R \approx 6$ (nevertheless one order of magnitude lower than ethanol and n-butanol). At 350°C the conclusions were qualitatively the same, but with lower responses (see Table I). Therefore, the best sensor's performance was recorded at 300°C, in which CdS proved its ability to selectively detect alcohols in complex mixtures.

3.2 Proposed gas sensing mechanisms

The main gas sensing feature of the prepared CdS sensors was the sensitivity to alcohols at all temperatures, with the response proportional to the length of the alcoholic chain. A possible

mechanism to explain this result is based on the dehydrogenation of the alcohol by the adsorbed oxygen ions. In the case of methanol, as the molecule approaches the oxygen-covered surface, it can lose one H from the CH_3 group and that of the OH group, due to the attraction with O^-_{ads}, resulting in the formation of a water molecule, which desorbs releasing one electron into the material. Thus, the dehydrogenated methanol turns into formaldehyde, the reaction schematics being the following:

$$CH_3OH + O^- \rightarrow CH_2O + H_2O + e^- \quad . \tag{2a}$$

A Lewis representation of the reaction of Eq. (2a) is sketched in Fig. 7a. A similar process can occur in the case of ethanol, which would turn into acetaldehyde, and in the case of n-butanol, which would turn into butyraldehyde, as in the following reaction schematics:

$$\begin{aligned} CH_3CH_2OH + O^- &\rightarrow CH_3COH + H_2O + e^- \\ CH_3CH_2CH_2CH_2OH + O^- &\rightarrow CH_3CH_2CH_2COH + H_2O + e^- \end{aligned} \quad . \tag{2b}$$

The huge increase in response between methanol (CH_3OH) and ethanol (CH_3CH_2OH) is probably due to the fact that in the case of ethanol, dehydrogenation occurs with one hydrogen from the CH_2 group instead of the CH_3 group, as represented in Fig. 7b. This is due to the higher electronegativity of CH_3 with respect to H, which attracts the shared negative charge more strongly, making the hydrogens of the CH_2 group more acid than those of CH_3. As a consequence, they have higher probability to react, indeed this is reflected in a higher sensor's response. The situation is similar in the case of n-butanol, where the hydrogens of the CH_2 group closest to the OH group are even more acid (reaction sketched in Fig. 7c). Since the difference in electronegativity between H and CH_3 is much higher than that between CH_3 and $CH_3CH_2CH_2$, the increase in probability of the first reaction in Eq. (2b) with respect to that of Eq. (2a) is much higher than the increase in probability of the second reaction in Eq. (2b) with respect to the first. This is in agreement with the observed differences in the sensor's response.

In addition to this phenomenon, it is reasonable to think that the efficiency of the reactions increases with the length of the alcoholic chain also because of the stronger attraction of the

molecule to the surface operated by the increasing number of hydrogen bonds that can be established between the surface and the hydrogens of the chain which are not involved in the reaction.

Regarding the other gases, we generally observed low responses, this being an indication of reactions with very low efficiency. An exception is represented by NO_2 at 250°C, which yields a response, in absolute value, of the same order of ethanol, but it decreases very rapidly with increasing temperature, reaching a very low value at the ideal alcohols detection temperature (300°C). The oxidizing behavior of all non-alcohols observed at 250°C was an effect of the slight humidity change caused by gas injection. Indeed, water vapor had an oxidizing effect on CdS, thus, even though this humidity change was very low, it was sufficient to hinder the weak reducing effect of the non-alcohols at this temperature.

4. Conclusions

In this work, we have described the synthesis of nanocrystalline CdS powder and its structural, morphological, thermal and optical characterizations. Conductometric gas sensors based on the as-synthesized CdS powder were fabricated by means of screen-printing technology. This sensing material has proved very peculiar selectivity towards alcoholic molecules with respect to many other interferes gases. Chemical reactions occurring at the surface offer possible explanation of the monotonic increase in the electrical response when increasing the length of the alcoholic chain. Possible applications of this result are of widespread interest, especially in those fields in which separation between alcohols and aldehydes is required, due to intrinsic selectivity of this material to these groups.

Acknowledgments

This work was supported by Programma Operativo FESR 2007-2013, Regione Emilia-Romagna – Attività I.1.1 and Spinner Regione Emila-Romagna.

References

[1] D. Shvydka, J. Drayton, A.D. Compaan, V.G. Karpov, Piezo-effect and physics of CdS-based thin film photovoltaics, Appl. Phys. Lett. 87 (2005) 123505.

[2] S.-L. Fu, T.-S. Wu, M.-P. Houng, The photoconduction mechanisms of screen-printed CdS films, Sol. Energ. Mater. 12 (1985) 309-317.

[3] I.J. Ferrer, P. Salvador, Photoluminescence and electroluminescence mechanisms at polycrystalline CdS in air and in contact with aqueous electrolytes, J. Appl. Phys. 66 (1989) 2568.

[4] R.R. Arya, P.M. Sarro, J.J. Loferski, Efficient cadmium sulfide on silicon solar cells, Appl. Phys. Lett. 41 (1982) 355.

[5] X. Jiao, L. Zhang, Y. Lv, Y. Su, A new acohols sesnor based on cataluminescence on nano-CdS, Sens. Actuators B 186 (2013) 750-754.

[6] R. Mishra, K. Rajanna, Metal-oxide thin film with Pd, Au andAg nanoparticles for gas sensing applications, Sensor Mater. 17 (2005) 433-440.

[7] R.A. Kadir, R.A. Rani, A.S. Zoolfakar, J.Z. Ou, M. Shafiei, W. Wlodarky, K. Kalantar-Zadeh, Nb_2O_5 Schottky based ethanol vapour sensors: Effect of metallic catalysts, Sens. Actuators B 202 (2014) 74-82.

[8] M.C. Carotta, M. Benetti, E. Ferrari, A. Giberti, C. Malagù, M. Nagliati, B. Vendemiati, G. Martinelli, Basic interpretation of thick film gas sensors for atmospheric application, Sens. Actuators B 126 (2007) 672-677.

[9] M.C. Carotta, A. Cervi, A. Giberti, V. Guidi, C. Malagù, G. Martinelli, D. Puzzovio, Metal-oxide solid solutions for light alkane sensing, Sens. Actuators B 133 (2008) 516-520.

[10] Y.-C. Liang, W.-K. Liao, X.-S. Deng, Synthesis and substantially enhanced gas sensitivity of homogeneously nanoscale Pd- and Au-particle decorated ZnO nanostructures, J. Alloy Compd. 599 (2014) 87-92.

[11] M.C. Carotta, A. Cervi, A. Giberti, V. Guidi, C. Malagù, G. Martinelli, D. Puzziovio, Ethanol interference in light alkane sensing by metal-oxide solid solutions, Sens. Actuators B 136 (2009) 405-409.

[12] A. Giberti, M.C. Carotta, B. Fabbri, S. Gherardi, V. Guidi, C. Malagù, High-sensitivity detection of acetaldehyde, Sens. Actuators B 174 (2012) 402-405.

[13] V. Guidi, M.C. Carotta, B. Fabbri, S. Gherardi, A. Giberti, C. Malagù, Array of sensors for detection of gaseous malodors in organic decomposition products, Sens. Actuators B 174 (2012) 349-354.

[14] X. Wang, S. Ji, H. Wang, D. Yan, Room temperature nitrogen dioxide chemresistor using ultrathin vanadyl-phtalocyanine film as active layer, Sens. Actuators B 160 (2011) 115-120.

[15] A. Giberti, B. Fabbri, A. Gaiardo, V. Guidi, C. Malagù, Resonant photoactivation of cadmium sulfide and its effect on the surface chemical activity, Appl. Phys. Lett. 104 (2014) 222102.

[16] Bruker AXS: TOPAS V4: General profile and structure analysis software for powder diffraction data. - User's Manual, Bruker AXS, Karlsruhe, Germany, 2008.

[17] R.W. Cheary, A.A. Coelho, A fundamental parameters approach to X-ray line-profile fitting, J. Appl. Crystallogr. 25 (1992) 109-121.

[18] R. W. Cheary, A.A. Coelho, J.P. Cline, Fundamental Parameters LineProfile Fitting in Laboratory Diffractometers, J. Res. Natl. Inst. Stand. Technol. 109 (2004) 1-25.

[19] A. Kern, A.A. Coelho, R.W. Cheary, Convolution based profile fitting. Diffraction Analysis of the Microstructure of Materials, edited by Mittemeijer, E.J. & Scardi, P. Materials Science, Springer, Germany, 2004.

[20] D. Balzar, Voigt-function model in diffraction line-broadening analysis. - Microstructure Analysis from Diffraction, edited by R. L. Snyder, H. J. Bunge, and J. Fiala, International Union of Crystallography, 1999.

[21] J. Winter, N. Gomez, S. Gatzert, C. Schmidt, B. Korgel. Variation of cadmium sulfide nanoparticle size and photoluminescence intensity with altered aqueous synthesis conditions. Coll. Surf. A 254 (2005) 147-157.

[22] A.I. Ekimov, Al.L. Efros, A.A. Onushchenko, Quantum size effect in semiconductor microcrystals, Solid State Commun. 56 (1985) 921–924.

[23] Y. Wang, N. Herron, Nanometer-sized semiconductor clusters: materials synthesis, quantum size effects, and photophysical properties, J. Phys. Chem. 95 (1991) 525-532.

Figure captions

Fig. 1: SEM image of a CdS film. Inset: EDX peaks with the results of the chemical analysis.

Fig. 2: XRD pattern of the as-synthesized CdS powder. The expected lines for β-CdS (space group F-43m) as in PDF card no. 80-0019 (calculated from ICSD no. 067789) are marked in blue.

Fig. 3: TG/DTG curves measured on the screen-printing paste obtained from the synthesized CdS powder.

Fig. 4: XRD pattern of the CdS powder after the thermal analysis. PDF cards of the identified crystalline phases marked as follows: i) red marks, monoclinic $CdSO_4$ (s.g. $Pn2_1m$), PDF no. 86-1558; ii) blue marks, orthorhombic $CdSO_4$ (s.g. Cmcm), PDF no. 77-2256; iii) green marks, $Cd_3O_2SO_4$ (s.g. Cm2a), PDF no. 032-0140: iv) light blue marks, cubic CdO (s.g. Fm-3m), PDF no. 005-0640.

Fig. 5: UV-Vis absorption spectra of the CdS powder.

Fig. 6: Absolute value of the responses of a CdS sensor to the target gases at the tested temperatures.

Fig. 7: Proposed sensing mechanism for alcohols: (a) methanol; (b) ethanol; (c) n-butanol. The arrow on the right of each reaction is a qualitative indication of the acidity of the hydrogen in red, which is proportional to the reaction probability.

Table(s)

Table I. Responses of a CdS sensor to the tested gases.

gas	methanol	ethanol	n-butanol	acetone	acetaldehyde	CH_4	SO_2	H_2	NO_2
conc. [ppm]	*5*	*5*	*5*	*10*	*10*	*2500*	*10*	*20*	*1*
250 °C	1.03	10	23	-0.22	-1.22	-0.02	-1.5	-0.09	-10.4
300 °C	7	63	90	1.2	6.02	0.12	0.44	0.27	-0.47
350 °C	5.4	35	69	0.56	3.4	0.12	0.3	0.06	0.25

Figure 1

Click here to download high resolution image

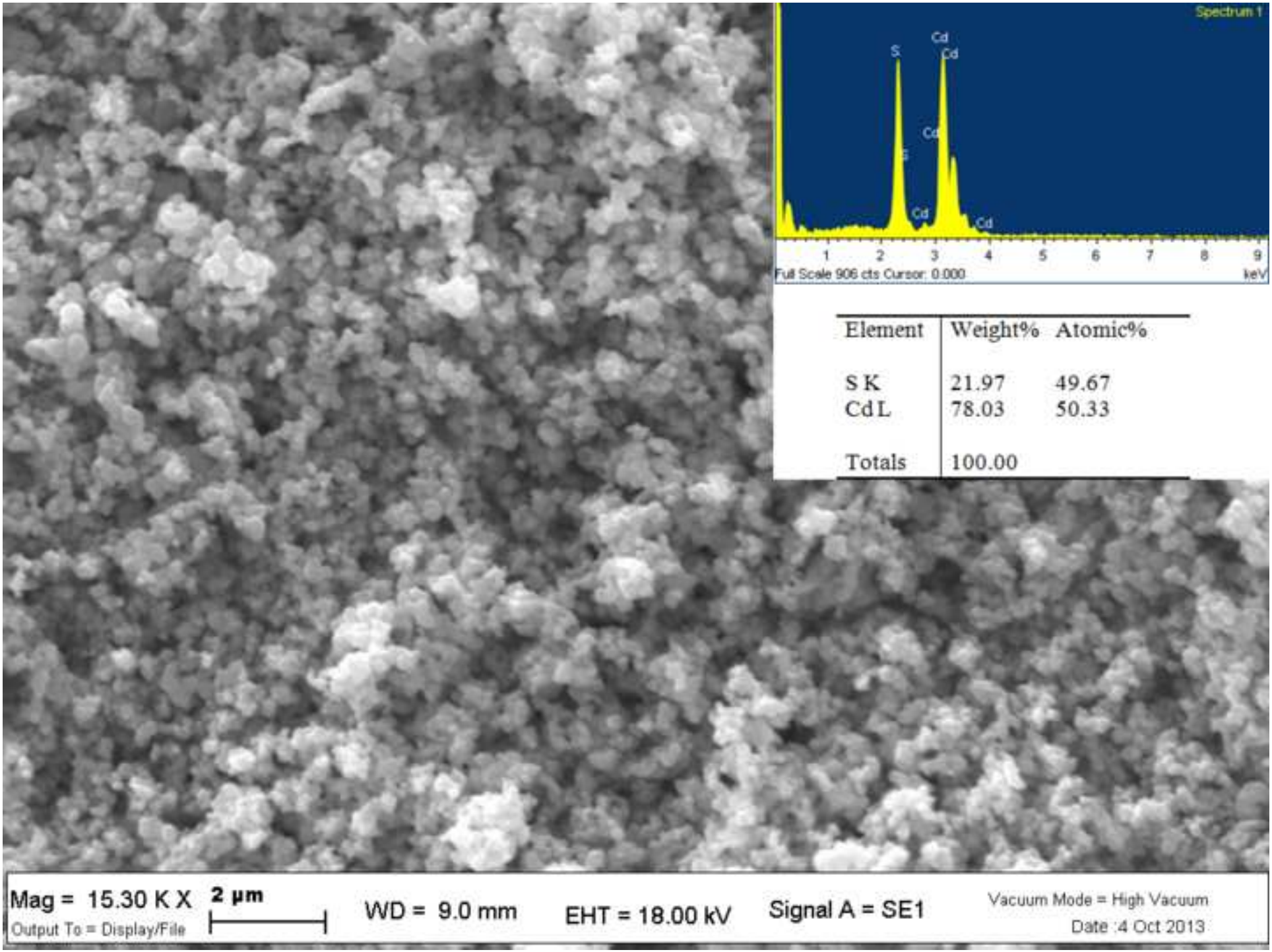

Figure 2

Click here to download high resolution image

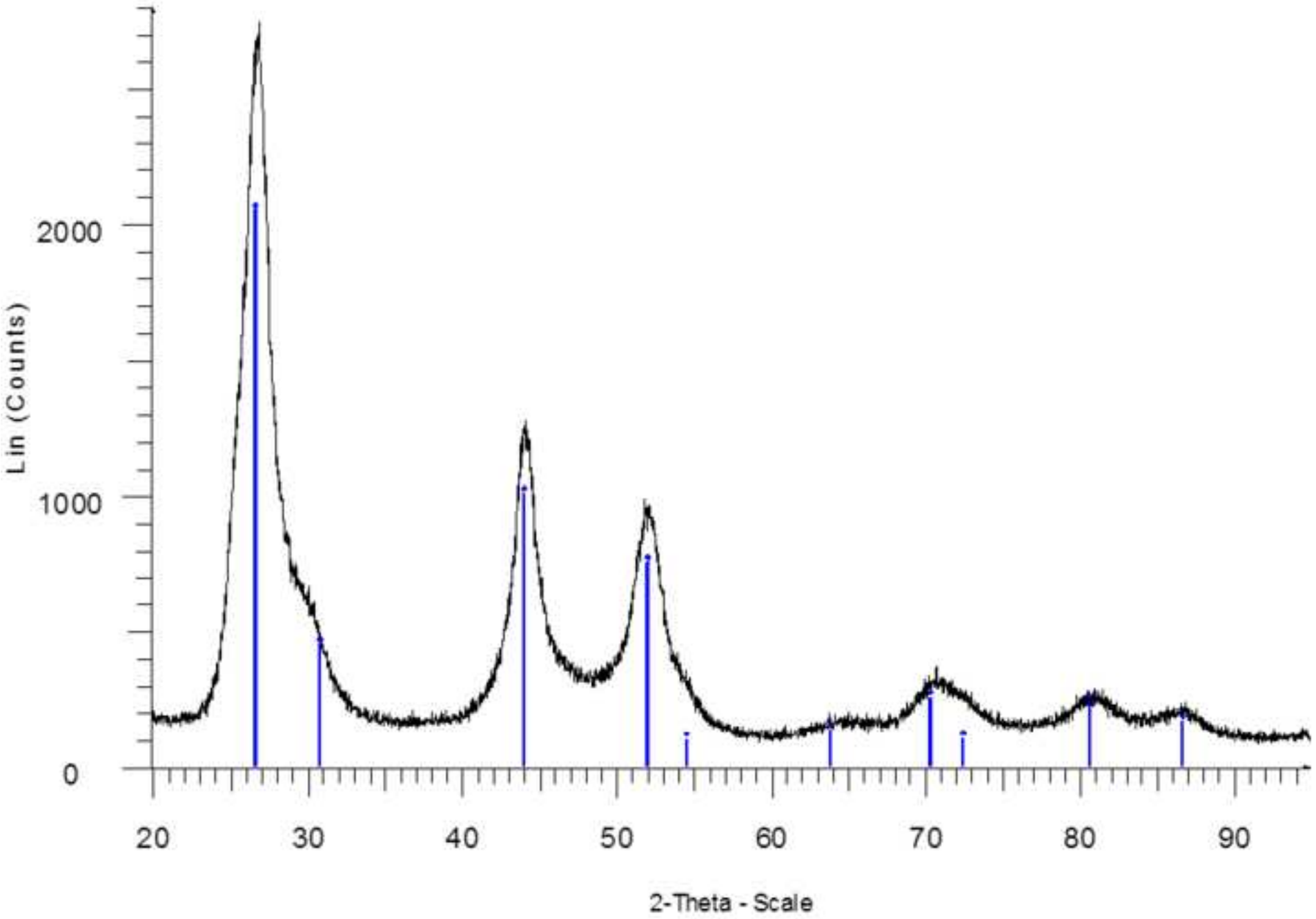

Figure 3

Click here to download high resolution image

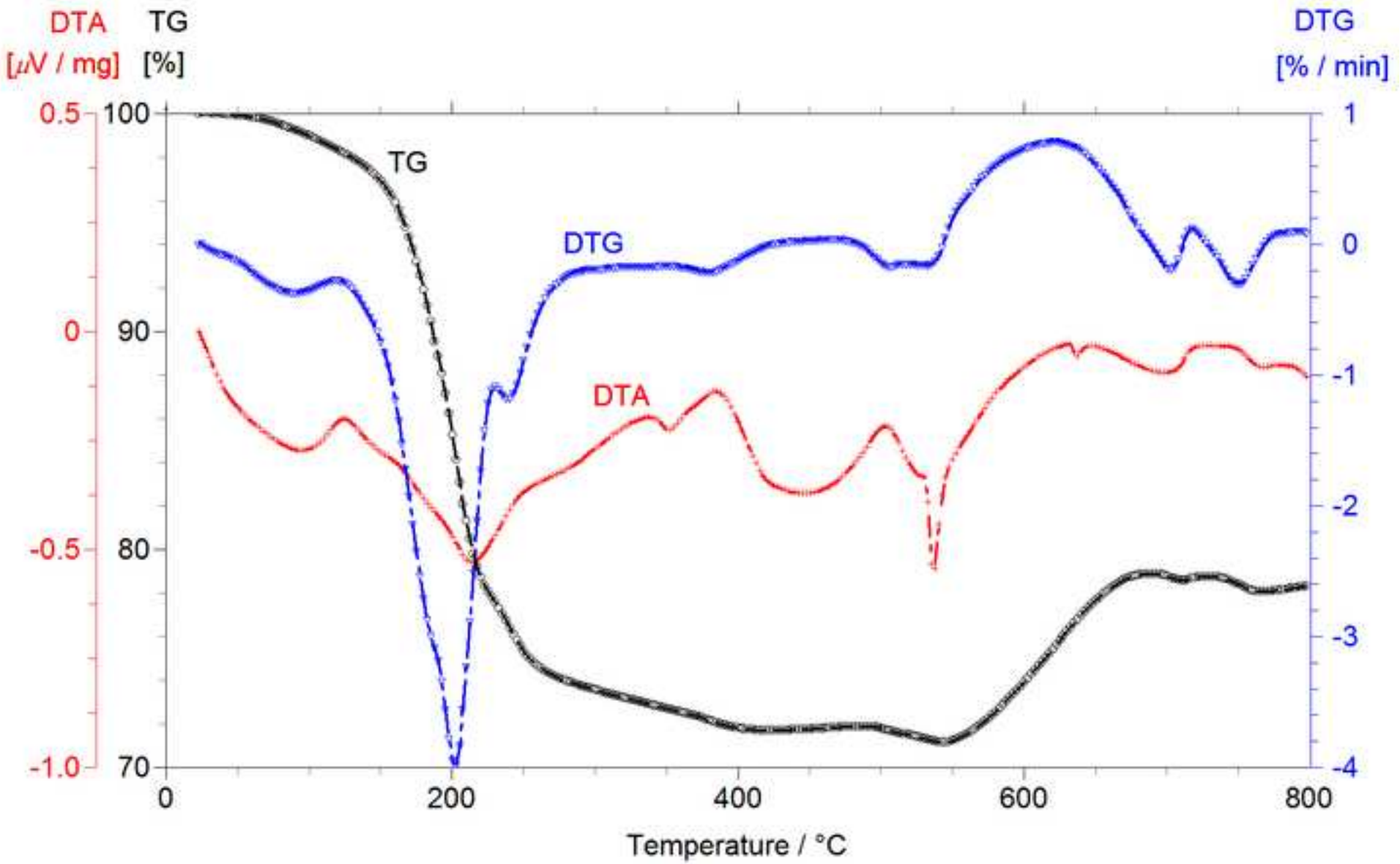

Figure 4

Click here to download high resolution image

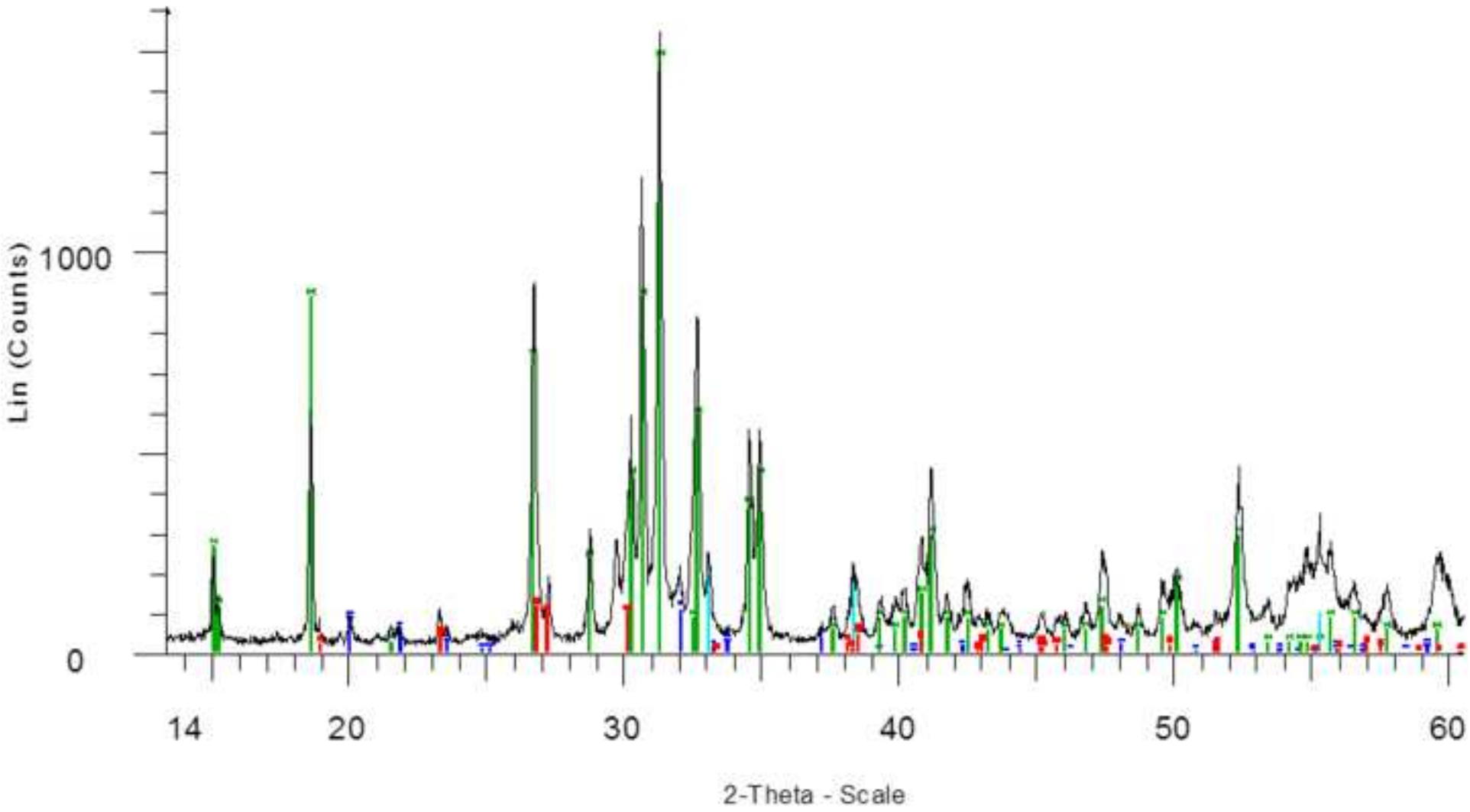

Figure 5

Click here to download high resolution image

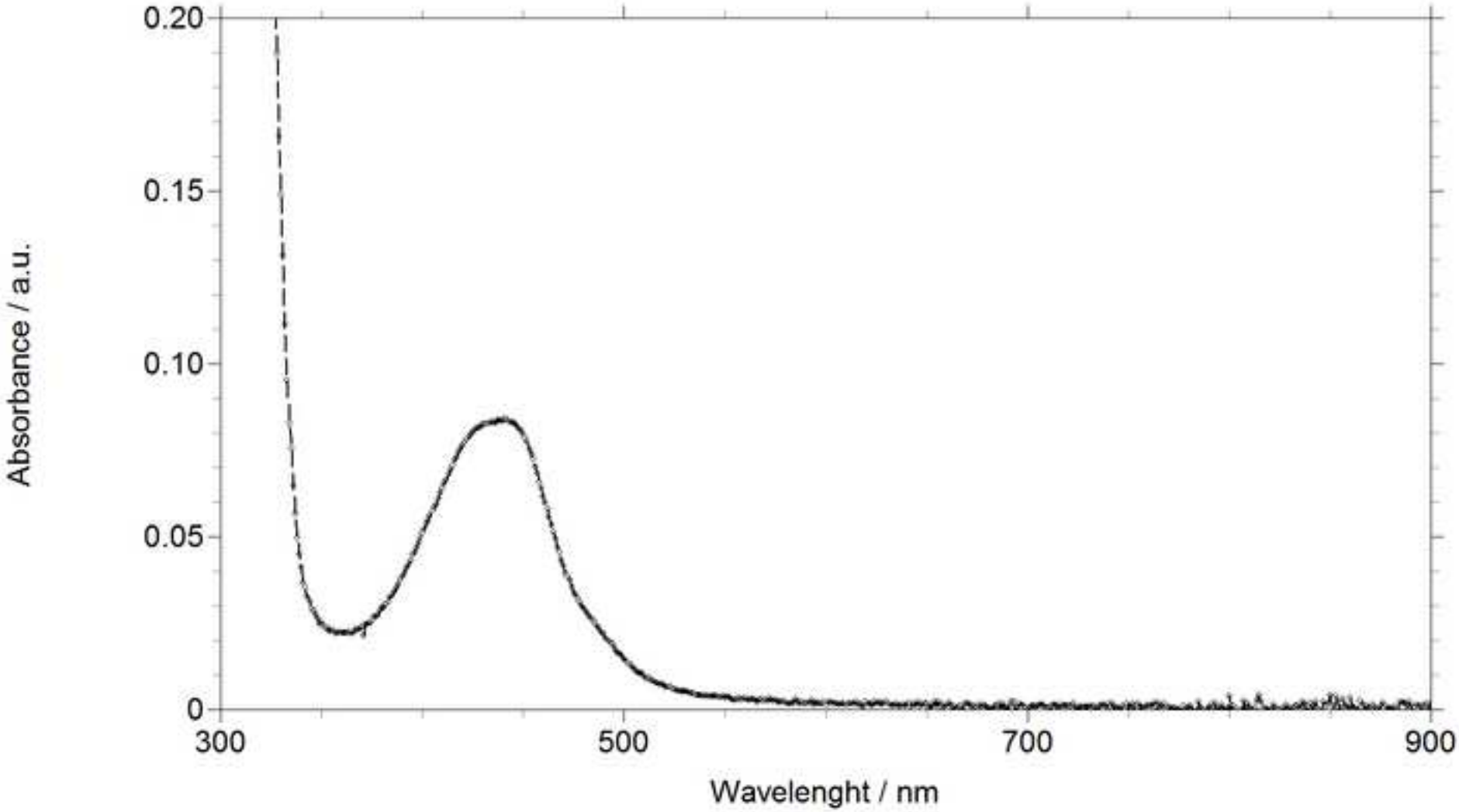

Figure 6

Click here to download high resolution image

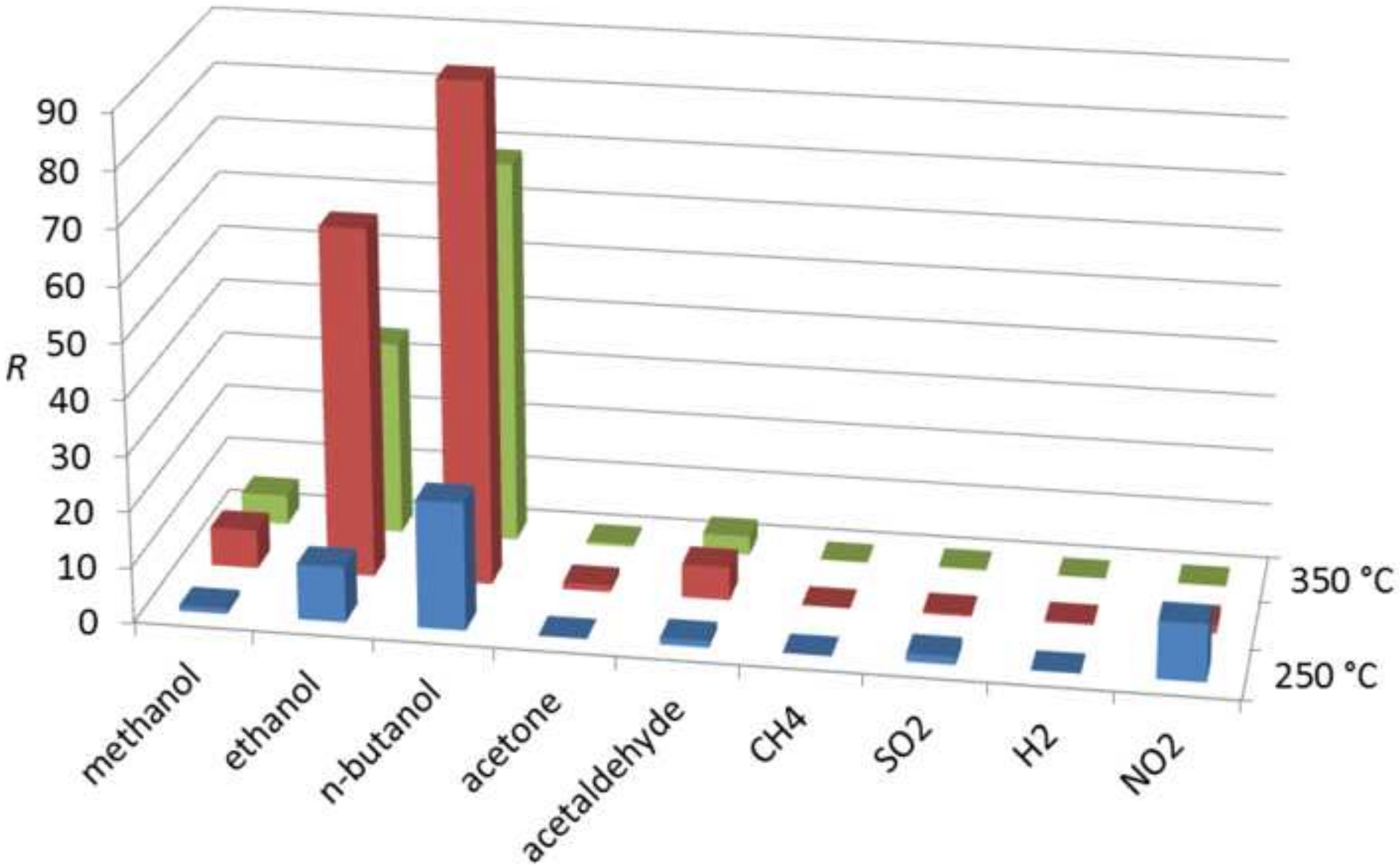

Figure 7

Click here to download high resolution image